Available online at www.sciencedirect.com

ScienceDirect

Procedia CIRP 104 (2021) 518–523

www.elsevier.com/locate/procedia

54th CIRP Conference on Manufacturing Systems

Detection of Defects in Solidified Layers within Laser-based Powder Bed Fusion using Active Thermography

Fabian Herzer[a,*], Franswa Abraham[a], Christoph Tammer[a], Georg Schlick[a], Christian Seidel[a,b], Johannes Schilp[a,c]

[a]Fraunhofer IGCV (Institute for Casting, Composite and Processing Technology), Am Technologiezentrum 10, 86159 Augsburg, Germany
[b]Department of Applied Siences and Mechatronics, University of Applied Siences Munich, Lothstr. 34, 80335 Munich, Germany
[c]University of Augsburg, Chair of Digital Manufacturing, Faculty of Applied Computer Sience, Eichleitnerstr. 30, 86159 Augsburg, Germany

* Corresponding author. Tel.: +49 821 90678-186; fax: +49 821 90678-199. *E-mail address:* fabian.herzer@igcv.fraunhofer.de

Abstract

During the metal-based additive manufacturing process „laser-based powder bed fusion“ (Short: PBF-LB/M) even minor deviations from the required process conditions, e.g. changes in the layer thickness or a reduction in the inert gas flow, can lead to defects and thus negatively affect the quality of the components. In the field of non-destructive testing, heat flow thermography is an established method for detecting defects close to the surface. In this paper, a method to investigate the potential of non-destructive testing by means of a laser as an excitation source for active thermography and the results for the material 1.4404 are presented.

Keywords: defect detection, active thermography, metal additive manufacturing, laser based powder bed fusion, laser beam melting

1. Introduction

After a decline in 2009, AM Industry has continued to grow steadily over the past decade. Over the past four years, the industry has grown by an average of 23.3 % [1]. It can be seen that machine manufacturers and service providers are increasingly offering solutions for the production of end products. This market segment requires higher quality standards compared to prototyping, for which additive manufacturing has been mainly used in recent years. [1]

The core challenge to enable market entry for end products in different sectors is still the conception of quality assurance along the process chain [2]. Additive manufacturing processes are capable of producing high quality products, but the technologies and their application are still hardly mature enough to guarantee this quality over a longer production period. One reason for this is the lack of process monitoring [1]. This has the greatest leverage for ensuring product quality, since in the area of quality assurance one of the greatest main of additive manufacturing, freedom of design, is also a major challenge. Non-destructive testing technologies, which can be used to detect process-related imperfections such as pores, cracks, delaminations or bonding defects in already manufactured components, reach their limits due to the complex structures or material properties, among other things. Only computer tomography (CT) is capable of investigating even complex structures. However, CT scans are both cost- and time-intensive and the technology also reaches its limits in terms of component size, material properties and resolution limit for the ability to detect relevant defects. [3, 4] For this reason, quality control is preferably performed whilst generating the part layer-by-layer during the manufacturing process. In addition to better accessibility to more complex structures and lower required inspection depths, this also has the advantage that if defects are detected early on, the

2212-8271
10.1016/j.procir.2021.11.087

manufacturing process of the affected components can be stopped, thus saving material costs and machine time.

During the metal-based additive manufacturing process laser-based powder bed fusion“ (Short: PBF-LB/M), thin layers of loose metal powder are selectively melted to build a three-dimensional component layer-by-layer [5, 6]. In order to achieve a well bonded metallic structure, the excess thermal energy of the molten bath typically re-melts a part of the already solidified material [7]. The possibilities of monitoring the PBF-LB/M process and thus the resulting quality of the components are shown in Figure 1.

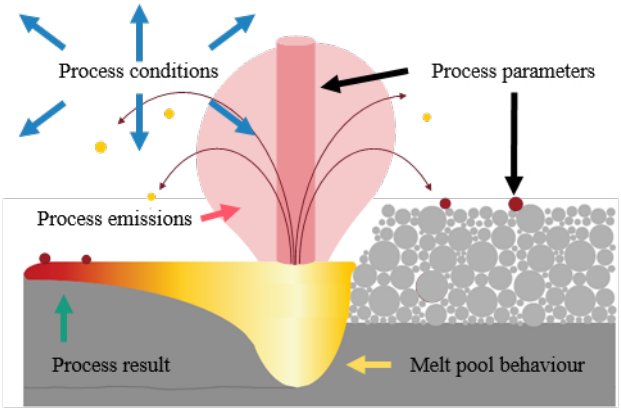

Fig. 1. Possibilities for process monitoring

In addition to monitoring process parameters, such as the laser power or the platform heating, the required process conditions, e.g. the residual oxygen content within the process chamber, must also be controlled. The next possible step in the monitoring chain is then to record and interpret the emissions generated by the manufacturing process. The different wavelength ranges can provide different information:

- The IR range can be used to draw conclusions about the behavior of the molten bath, for example, and
- the UV range can provide information about the elemental composition of the molten material [8, 9].

The last possible step to ensure the component quality within the manufacturing process is the control of the process result, in this case the solidified layer.

2. State of the Art: In-Process Defect Detection

There are already various approaches for detecting potential errors due to minor deviations in the process parameters or process conditions used during the process. Whether a technology is suitable for such an application must be derived from the characteristics and causes of the individual defects. Therefore, the different defect categories as well as the technologies used for detection and the approaches using thermography are presented below.

2.1. Selected Defect Causes and Categories

In the field of standardisation, there is currently no approved standard describing the various types of defects by their causes and characteristics. However, there are already various projects that have taken up this topic [3, 4, 10, 11]. The causes for the different defects can be divided in following categories: machine (e.g. laser, recoater, scanner), material (e.g. age or oxidation), human (e.g. handling, cleaning, part design) and process (e.g. remaining O_2, parameters) [3, 10]. With regard to defects, a distinction can generally be made between geometric deviations, surface quality, building and internal defects [4, 11]. Table 1 shows selected internal defects and their description:

Table 1: Selected Internal Defects [3, 11]

Defect	Description
Cracks	Cracks can be within the component or more commonly a disconnection of the part from the build platform is seen.
(Gas) Pores	Entrapped gas pores within the bulk of material. Material dependent.
Lack of Fusion	Lack of fusion (pores) in between layers.
Inclusions	Embedded contaminations from powder or equipment

2.2. In-situ Monitoring

In general, the technologies used can be assigned to the corresponding objects of observation. The technologies discussed below are mainly concerned with recording process emissions and controlling the process step of powder application [3]. These can be further divided into the areas on-axis (or co-axial) and off-axis due to their process access. On-axis in this context means that the technologies are integrated into the beam path of the laser unit in order to detect the process emissions directly during melting at that particular point. Off-axis, on the other hand, means that the technologies used are mounted at a certain angle to the building plate and detect it over a large area.

In addition to the features already mentioned, the decisive difference between the individual technologies is the wavelength range used. Cameras in the visible to NIR range are used, for example, to detect irregularities in the powder application [12], the component quality based on the resulting surface properties [13] or the melt pool geometries [14]. Pyrometers and thermographic cameras in the NIR to LWIR range, on the other hand, are used, for example, to record melt pool temperatures [15], to record temperature profiles of the scan track [8, 16] or to identify ejections form the melt pool such as spatters [17]. With the exception of systems for powder bed monitoring, where a flash is used to better illuminate the installation space [12], the monitoring technologies used passively record the heat introduced by the melting process.

2.3. Thermography for In-situ sensing

Infrared thermography uses the fact that all objects above absolute zero emit electromagnetic radiation, so-called thermal radiation [18]. Infrared systems can measure, process and visualize this heat radiation from surfaces without contact [19]. In general, thermography can be used in two different ways to detect internal, near-surface defects: passive and active [20]. Figure 2 illustrates how the defects in both application forms are reflected in the resulting thermogram:

In the passive form, the heat inherent in the process is recorded. If this heat hits a defect on its way to the part surface, the cooling process is delayed, and the corresponding area appears darker in the thermogram. If, on the other hand, the heat is actively introduced from outside, it accumulates on the defect as it flows into the inside of the part, is reflected and appears as a bright spot in the thermogram [21].

As already mentioned, thermography is mainly used for monitoring the process signatures passively [8, 22]. Active approaches, using an external heat source to detect near-surface defects, are so far only used after the process [23–26].

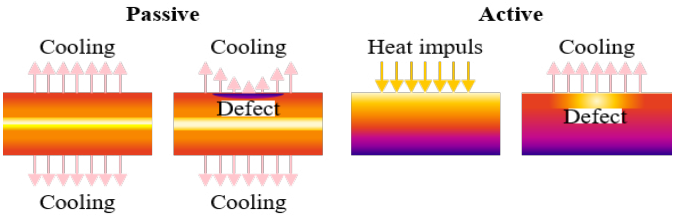

Fig. 2. Heat flow for passive and active thermography

3. Proposed Methodology

In order to determine whether the process laser is suitable for this application, this chapter presents the integration of thermography in a PBF-LB/M system and a method for investigating the potential of the system laser as an excitation source for active thermography.

3.1. Integration of the Thermography

An AconityOne laser PBF-LB/M system was used for all test series. To be able to access the building platform with a thermography camera, an integration module was developed and implemented (Figure 3). In order to make the viewing angle as steep as possible to keep the distortion in the image as low as possible, the working area for the laser was reduced from 400 mm to 200 mm in diameter. This allowed the camera to be placed at an angle of 65° to the building platform. In all tests a quantum detector camera of the type FLIR SC5650 (detector size 640 x 512 pixels, maximum frame rate in full frame 100 Hz, waveband 2.5 - 5.1 µm) was used.

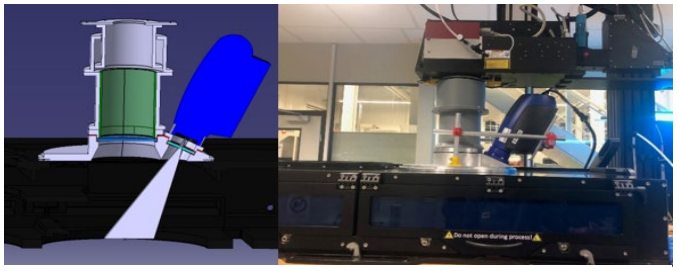

Fig. 3. Integration module for the AconityOne

3.2. Procedure

The following steps were defined for the systematic approach to explore the potential of the technology and gradually approach the real defect sizes.

3.2.1. Definition of suitable test defects

The minimum defect size, which can be detected by active thermography, is bound to the following physical law:

$$Minimum\ detectable\ Defect\ size \geq Defect\ depth \quad (1)$$

For this reason, thermography is only suitable for the detection of lack of fusion defects, as these can have sizes from 50 to 500 µm [11]. To be able to prove the general detectability of near-surface defects in the first step, the defects must have the following characteristics:

- Fixed position: This is important in order to assign the resulting signal to a defect.
- Realistic: The inserted defect must have the same characteristics as real lack of fusion defects in order to cause a comparable reaction behaviour.
- Existing: The defects must remain in the part after remelting of the overlying layers.

3.2.2. Determination of suitable excitation parameters

For the determination of the excitation parameters, criteria were also defined which are to be considered from the point of view of the manufacturing process and the detection process:

- Minimal heat input: In order to change the microstructure as little as possible, the heat input must be as low as possible, but must allow thermographic detection.
- Excitation over the complete component area: To ensure that scans do not end in the middle of the component and thus do not reach potential defects, the scan must cover the entire width of the component.
- Unidirectional excitation: Bidirectional excitation at the end of a scan would cause the neighbouring scan to start at this point and lead to temperature peaks that would be very difficult to distinguish from defects.

3.2.3. Recording of the thermographic reaction

Within the last step of the procedure, the thermographic reaction has to be recorded and interpreted. For this purpose, the reaction behaviour of the defects must be compared with defect-free areas of the component and analysed with regard to the differences in contrast. On the basis of the analysis results, the next steps are then determined, which are either an adjustment of the detection parameters (framerate and integration time) or directly the next step to reduce the defect sizes in order to gradually approach the real defects.
The procedure and the individual possible iteration loops are illustrated in the following graphic:

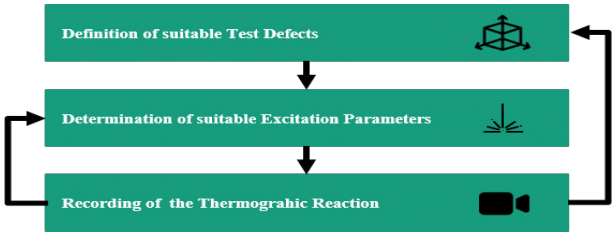

Fig. 4. Developed iterating procedure

4. Case study

This chapter shows the results of applying the procedure for the material 1.4404. The production of all test samples was carried out with standard parameters (laser power: 214 W, scanning speed: 928 mm/s, layer thickness 0.04 mm and hatch distance 0.1 mm). For the analysis of the micro sections, all

samples were etched after polishing (etching agent: Adler etch, etching time: 25 s).

4.1. Determination of suitable defect size

To fulfil the criteria mentioned in chapter 3.2.1, test specimens with different defect sizes were produced and then vertical and horizontal microsection were analysed. The choice of the defect sizes was based on already investigated sizes for the material AlSi10Mg [27]. Following, ellipse formed sizes were printed in 10 x 10 mm cubes:

Table 2. Investigated defect sizes

Defect Number	Dimensions of Defects	
	Major Radius (µm)	Minor Radius (µm)
1	500	150
2	450	125
3	400	100
4	350	75
5	300	50

In addition to the defect sizes, another criterion was examined in this test series, namely the necessary defect depth. If the selected defects are placed too close to the surface, the melt pool sinks, and the defects are clearly visible on the surface. This means that the formation of hotspots may not be due purely to the thermal reaction from inside the component, but also to the interaction of the excitation source with the surface. This should therefore be avoided for this investigation.

Based on the vertical and horizontal microsection together with the visual impression of the surface, the following characteristics for the artificially introduced defects were found:

- Defect width: 350 to 500 µm
- Defect height: 120 µm
- Defect depth: 160 µm

Figure 5 presents an example for a horizontal micrograph of defect width 400, 450 and 500 µm (right to left) and a defect height of 120 µm:

Fig. 5. Horizontal micrograph of artificially inserted defects

Lack of fusion defects provoked directly during production, e.g. by reducing the inert gas flow [28], cannot serve as test artefacts, as they do not meet criterion 1 or will most probably not meet criterion 3. In order to make initial detection easier in the subsequent steps, no individual defects in the form of ellipses were inserted into the components, but rather elongated defects with the specified height and depth, and widths of 300, 400 and 500 µm (Figure 7).

4.2. Determination of suitable excitation parameters

The energy input while using the laser beam as an excitation source is mainly determined by the two parameters laser power and scanning speed. In order not to change the microstructure of the parts, the maximum scanning speed as well as the lowest possible laser power was defined as the starting point and the power was gradually increased in a test series. Ex-situ preliminary investigations [25] and other state of the art work [23] had already shown that the reaction behaviour of the defects is to be expected in the low ms range and that the scanning speed should therefore be set as high as possible.

Table 3. Parameter combinations

Parameter Combination	Laser Power [W]	Scan Speed [mm/s]
1	40	5000
2	45	5000
…	…	….
15	110	5000
16	120	5000
…	…	…
19	150	5000

The minimum laser power is determined by the dynamic application range of fibre lasers from 10 to 100%. The laser of the AconityOne has a maximum power of 400 Watt, which results in the 40 Watt used for the minimum power. In order to better analyse the possible melt pools resulting from the parameter combinations shown, no test cubes with complete layers were built up, but individual tracks (three tracks per parameter combination) were exposed on solid 1.4404 material. To ensure that the surface roughness of the solid material is as comparable as possible to additively build up parts, the smooth surface was blasted with sand before exposure, how it is performed in the usual pre-processing of a building plate. After performing the single-track exposure, the vertical microsection where etched and analysed.

The analysis of the single tracks showed that already the combination with the lowest energy input leads to a melt pool depths of 0.031 to 0.041 mm. With increasing laser power no increase of the melt pool depth could be detected, which is due to the high scanning speed. This remelting needs to be examined more closely in further experiments and the effects on the mechanical properties must be investigated. However, *Yasa et al* have already been able to identify positive effects with 1.4404 through their work on remelting. They were able to increase density by reducing porosity and also achieved enhanced surface properties [29, 30].

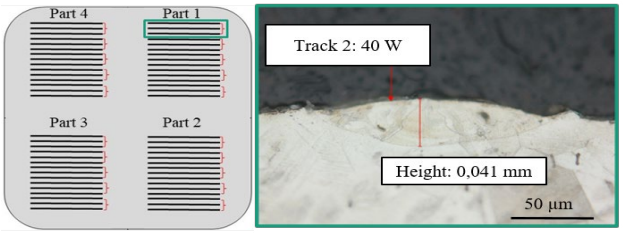

Fig. 6. Single track test with melt pool analysis for 40 W

To meet the already defined criteria 2 and 3, the scanning strategy of the standard parameters was adjusted in Netfabb as follows:

- Modus: Stripes changed to hatches
- Hatch length > part dimensions

- Starting angle for hatches: 90-degree angle to the defect strips
- Hatch distance: 0.100 and 0.200 mm

4.3. Thermographic Detection

In order to be able to test the parameter combinations already used for the single tracks for excitation, test cubes were designed, which consist of individual layer stacks. Each stack always consists of 5 defect layers, 4 cover layers, the analysis layer and 5 intermediate layers. In Figure 7 the structure of these defect cubes is illustrated.

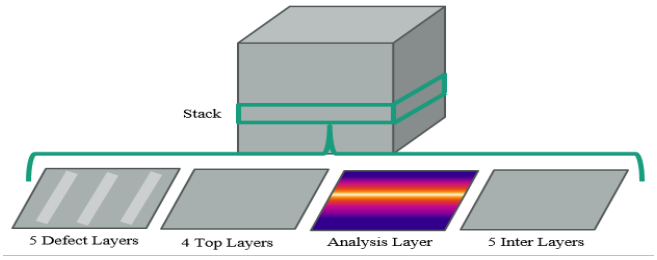

Fig. 7. Defect cubes with stacks

At the beginning, 50 full layers were built up in order to be able to separate the samples from the build platform afterwards. After building up the 5 defect and 3 surface layers, the last surface layer was exposed manually to prevent the application of the next powder layer. For the analysis layer, a switch from the printing parameters to the analysis parameters was performed and the exposure with the thermographic camera was recorded. The following parameters were used:

- Resolution: 256 x 192 Px
- Frame rate: 497 Hz
- Integration time: 0.001 s

The reduction of the used detector section was carried out in order to achieve the highest possible temporal resolution of the reaction behaviour. This resulted in a detectable area of the construction panel of 450 x 250 mm, which made it possible to place 8 cubes with 10 x 10 mm in the field of view. The integration time was determined by pre-tests in order to avoid overexposure of the detector, which would have made an analysis of the thermograms impossible. Within each construction job, two pairs of cubes were provided for analysis using the different hatch distances 0.100 and 0.200 mm and the 19 different laser powers were divided between these two pairs. The analysis of the respective thermograms did not take place directly after the exposure, but after the test execution. Since the integration of active thermography was previously only done in hardware but not in software, exposure and recording had to be triggered manually. In order to be able to compare the reaction behaviour of selected areas nevertheless, so-called ROIs (region of interests) with a size of 3 x 3 pixels were placed at the same places within the thermograms by orienting them to the outer contours of the cubes. Using the start of exposure within a video sequence, the reaction behaviour at the same point in time was then extracted over the number of images.

In the first step, the general detectability of all three defect sizes was investigated. Even with the lowest laser power of 40 W, hotspots appeared in the recorded thermograms at the corresponding points. Figure 8 shows the intensity maximum for the defect with the size of 400 µm. This stands out clearly from the direct surroundings. The other two defects are also visible but have lower intensities. This is due to the fact that the defect with 300 µm has already cooled down somewhat at this point and the heat accumulation is only formed at the defect

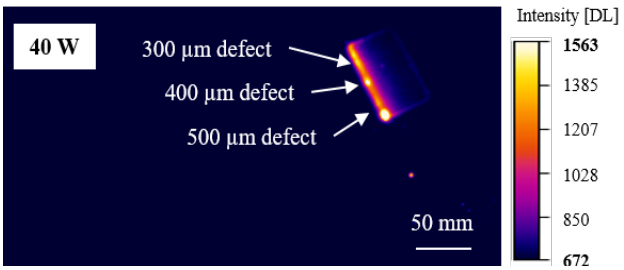

Fig. 8. Thermogram with 40 W laser power and 0.100 hatch distance

with 500 µm.

In the next step, the influence of higher laser power on contrast formation, the difference between a defect and the defect-free environment, was analysed. It was found that increasing the laser power also increases the contrast.

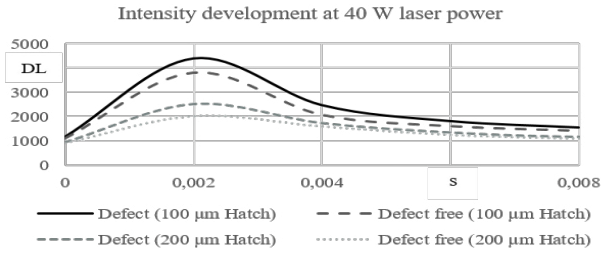

Fig. 9. Intensity Development with different hatch distances

The largest increase in contrast can be observed between 40 and 80 W. Above 80 W, the contrast continues to increase, but the increase is significantly lower. In future investigations it is therefore necessary to further analyse in detail the effects of increased laser power on the mechanical properties in order to define the final inspection laser power both via thermographic detection and via component properties.

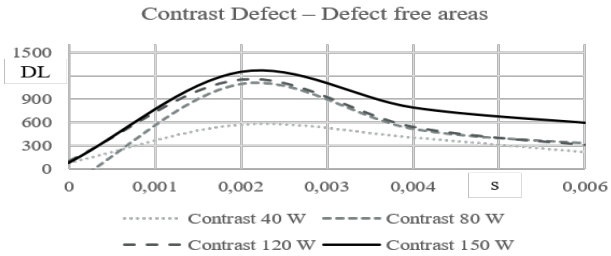

Fig. 10. Contrast Development with increasing laser power

By increasing the hatch spacing, the overlapping of heat-affected zones of adjacent scans should be reduced, thus increasing contrast. On the basis of the results, this behaviour could not be determined. The reason for this could be that the defect was not hit correctly. According to this, in order to reduce the overlap of heat affected zones, it would not be necessary to reduce the hatch distances, but rather to delay the scans. This has to be checked in case of further iteration loops.

5. Conclusion and Outlook

Within the scope of this work, the detection of local imperfections or defects is addressed. A procedure is presented

to explore the potential of the system laser as an excitation source for the detection of local defects in solidified layers using active thermography and this procedure was validated for a PBF-LB/M system of type AconityONE using a self-developed integration module. On the basis of the test results, the basic detectability of the defects introduced after excitation by the system laser could be proven. Furthermore, the laser powers of 40 to 80 W were found to be best suited for excitation. Larger hatch distances reduced the generation of hotspots that were not caused by defects, but they reduced the contrast formation between defect and defect free areas.

In the next steps, the investigated defect shapes are to be adapted step by step to real lack of fusion defects (oval with lengths of 100 to 300 µm), the corresponding reaction behaviour is to be recorded and, if necessary, the scanning strategy is to be adapted. Based on this, suitable image processing methods must then be identified that enable automated detection of these defects in the thermograms. In particular, research will be conducted to determine whether conclusions can be drawn about the defect sizes based on the temperature peaks in combination with the defect shape in the thermograms.

Acknowledgements

The authors express their sincere thanks to the Land of Bavaria and its Bavarian Ministry of Economic Affairs, Regional Development and Energy StMWi for funding the "MULTIMATERIAL-Zentrum Augsburg" (English: “Multi-material Center Augsburg”). Furthermore, the authors thank Norbert Zimmer for the support while conducting the experiments.

References

[1] T. Wohlers *et al., Wohlers report 2020: 3D printing and additive manufacturing state of the industry*. Fort Collins, Colo.: WOHLERS Associates, 2020.

[2] E. Witt and C. Anton, Eds., *Additive Fertigung: Entwicklungen, Möglichkeiten und Herausforderungen: Stellungnahme*. Halle (Saale), Mainz, München: Deutsche Akademie der Naturforscher Leopoldina e.V. - Nationale Akademie der Wissenschaften; Union der deutschen Akademien der Wissenschaften e. V; acatech - Deutsche Akademie der Technikwissenschaften e. V, 2020.

[3] M. Grasso and B. M. Colosimo, “Process defects and in situ monitoring methods in metal powder bed fusion: a review,” *Meas. Sci. Technol.*, vol. 28, no. 4, p. 44005, 2017.

[4] B. Dutton, M. H. Rosli, and D. Ross-Pinnock, “NDT Standards for Additive Manufacturing,” Grenoble, Apr. 10 2018.

[5] S. Negi, S. Dhiman, and R. Kumar Sharma, “Basics and applications of rapid prototyping medical models,” *Rapid Prototyping Journal*, vol. 20, no. 3, pp. 256–267, 2014.

[6] I. Yadroitsev *et al.,* “Strategy of manufacturing components with designed internal structure by selective laser melting of metallic powder,” *Applied Surface Science*, vol. 254, no. 4, pp. 980–983, 2007.

[7] L.-C. Zhang *et al.,* “Review on manufacture by selective laser melting and properties of titanium based materials for biomedical applications,” *Materials Technology*, vol. 31, no. 2, pp. 66–76, 2016.

[8] M. A. Doubenskaia *et al.,* “Determination of True Temperature in Selective Laser Melting of Metal Powder Using Infrared Camera,” *MSF*, vol. 834, pp. 93–102, 2015.

[9] A. R. Nassar, T. J. Spurgeon, and E. W. Reutzel, “Sensing defects during directed-energy additiv manufacturing of metal parts using optical emissions spectroscopy,”

[10] T. Schlauf, M. Lutter-Günther, and C. Rosenkranz, “Project report – AM 4 Industry - LBM Additive Manufacturing Defect Catalogue,” 2019.

[11] S. Everton *et al.,* “Identification of Sub-Surface Defects in Parts Produced by Additive Manufacturing, Using Laser Generated Ultrasound,” *Materials Science & Technology*, 2016.

[12] B. K. Foster *et al.,* “Optical, layerwise monitoring of powder bed fusion,” in *Solid Freedom Fabrication Symposium Proceedings 2015*, pp. 295–307.

[13] J. Zur Jacobsmuhlen *et al.,* “High resolution imaging for inspection of laser beam melting systems,” in *2013 IEEE International Instrumentation and Measurement Technology Conference (I2MTC)*, Minneapolis, MN, May. 2013 - May. 2013, pp. 707–712.

[14] T. Craeghs *et al.,* “Determination of geometrical factors in Layerwise Laser Melting using optical process monitoring,” *Optics and Lasers in Engineering*, vol. 49, no. 12, pp. 1440–1446, 2011.

[15] I. Yadroitsev, P. Krakhmalev, and I. Yadroitsava, “Selective laser melting of Ti6Al4V alloy for biomedical applications: Temperature monitoring and microstructural evolution,” *Journal of Alloys and Compounds*, vol. 583, pp. 404–409, 2014.

[16] M. Montazeri and P. Rao, “Sensor-Based Build Condition Monitoring in Laser Powder Bed Fusion Additive Manufacturing Process Using a Spectral Graph Theoretic Approach,” *Journal of Manufacturing Science and Engineering*, vol. 140, no. 9, p. 216, 2018.

[17] B. Lane *et al.,* “Thermographic Measurements of the Commercial Laser Powder Bed Fusion Process at NIST,” *Rapid Prototyping Journal*, vol. 22, no. 5, pp. 778–787, 2016.

[18] M. F. Modest, *Radiative heat transfer,* 3rd ed. New York: Academic Press, 2013.

[19] X. P. V. Maldague, *Theory and practice of infrared technology for nondestructive testing*. New York, NY: Wiley, 2001.

[20] C. Ibarra-Castanedo *et al.,* “Active infrared thermography techniques for the nondestructive testing of materials,” in *Ultrasonic and Advanced Methods for Nondestructive Testing and Material Characterization*, C. H. Chen, Ed.: WORLD SCIENTIFIC, 2007, pp. 325–348.

[21] J. Aderhold and P. Meinlschmidt, “Grundlagen der Thermografie,” in *Vision Leitfaden*, vol. 12, *Leitfaden zur Wärmefluss-Thermographie: Zerstörungsfreie Prüfung mit Bildverarbeitung*, M. Sackewitz, Ed., Stuttgart: Fraunhofer-Verl., 2011, pp. 8–11.

[22] H. Krauss, “Qualitätssicherung beim Laserstrahlschmelzen durch schichtweise thermografische In-Process-Überwachung,” Dissertation, Herbert Utz Verlag GmbH.

[23] B. Zhang *et al.,* “Detection of Subsurface Defect for Metal Additive Manufacturing Using Flash Thermography,” in *2018 ASPE and euspen Summer Topical Meeting on Advancing Precision in Additive Manufacturing*, American Society for Precision Engineering (ASPE), Ed., Berkeley, California, USA, 2018, pp. 121–126.

[24] X. Zhang *et al.,* “Quality Control of Additively Manufactured Metallic Structures with Machine Learning of Thermography Images,” *JOM*, vol. 92, no. 3, p. 112, 2020.

[25] F. Herzer and J. Schilp, “Aktive Thermografie als In-Prozessüberwachungsmethode für Selektives Laserstrahlschmelzen,” in *DGZfP-Berichtsband BB 173*, Halle (Saale), 2019.

[26] C. G. Kolb, F. Bayerlein, and M. F. Zaeh, “Prozessüberwachung des Laserstrahlschmelzens mittels aktiver Thermografie: eine ex-situ sowie in-situ Machbarkeitsstudie,” in *Rapid.Tech + FabCon 3.D – International Trade Show + Conference for Additive Manufacturing*, M. Kynast, M. Eichmann, and G. Witt, Eds., München: Carl Hanser Verlag GmbH & Co. KG, 2018, pp. 182–197.

[27] S. Kleszczynsk and G. Witt, “Einfluss lokaler Fehlstellen auf die statische Festigkeit laser-strahlgeschmolzener Bauteile,” in *Fachtagung Werkstoffe und Additive Fertigung: 25.-26.04.2018, Potsdam: Tagungsband*, P. Hoyer, Ed., pp. 206–213.

[28] A. Ladewig *et al.,* “Influence of the shielding gas flow on the removal of process by-products in the selective laser melting process,” *Additive Manufacturing*, vol. 10, pp. 1–9, 2016.

[29] E. Yasa and J. P. Kruth, “Application of laser re-melting on selective laser melting parts,” *Advances in Production Engineering & Management*, no. 4, pp. 259–270, 2011.

[30] E. Yasa, J. Deckers, and J.-P. Kruth, “The investigation of the influence of laser re-melting on density, surface quality and microstructure of selective laser melting parts,” *Rapid Prototyping Journal*, vol. 17, no. 5, pp. 312–327, 2011.